Florida State University Libraries

2016

Constraints on the Strange Quark Parton Distribution Function from Weak Vector Boson Production

Dayshon Tyree Mathis

FLORIDA STATE UNIVERSITY

COLLEGE OF ARTS AND SCIENCES

Constraints on the Strange Quark Parton Distribution
Function from Weak Vector Boson Production

By

Dayshon Mathis

Research Advisor

Dr. Joseph Francis Owens III

Semester Defense

Summer Semester, year 2016

The members of the Defense Committee approve the thesis of Dayshon Mathis defended on July 21, 2016.

Thesis Director: Dr. Joseph Francis Owens III

Outside Committee Member: Dr. Mark Sussman

Committee Member: Dr. Takemichi Okui

Contents

Abstract

The Standard Model is a useful theory due to its predictive capabilities. Hadrons, as described by Standard Model, consist of quarks and gluons, collectively called partons. However, there is no theory that provides an exact state of a parton within a hadron. The properties associated with partons currently must be gained empirically. This is done by fitting free parameters in models with data from a number of different experiments. The Parton Distribution Functions (PDFs) corresponding to the up, down, antiup, and antidown quarks and the gluon have been well constrained since they are the lightest partons. The next lightest quark distribution, the strange-antistrange PDF, is the subject studied here. Using the most recent CTEQ-Jefferson Lab (CJ15) PDF set as a starting point and analysing new data sets sensitive to the strange quark PDFs one could determine constraints for the strange PDF. Experiments with a center-of-mass energy, $\sqrt{s}$, of 7 TeV data from the Compact Muon Solenoid (CMS) and 8 TeV Large Hadron Collider b (LHCb) detectors is analysed as a means of gaining constraints. However, the addition of these data sets to the original CJ15 data sets are not significant enough to support changing the strange distribution. Additional factors dependent on the momentum fraction, x, are added to the original CJ15 parameters and the addition of these factors are partially supported by the additional data sets, still more research is needed. The addition of new data sets with observables sensitive to the strange quark such as $W + c$ final state

3

data at the Large Hadron Collider (LHC) may need to be considered to gain further constraints of the strange PDF.

Standard Model										
Fermions						Bosons				
Quarks			Leptons							
1st	2nd	3rd	1st	2nd	3rd					
u	c	t	e	μ	τ	γ	g	$W^{\pm}$	Z^0	H^0
d	s	b	ν_e	ν_μ	ν_τ					

Table 1: This table contains the particles known to the Standard Model, excluding the antiparticles. The quarks and leptons are broken up into generations. The generations are distinct in their mass ranges. The first generation is lighter than the second generation and the second lighter than the third. The first row of quarks contains the up quark, the charm quark and the top quark. These quarks have charge $+\frac{2}{3}$ and the row below it contains the down quark, the strange quark and the bottom quark. These quarks have charge $-\frac{1}{3}$. The first row for the lepton column are the charge leptons. They have charge -1, while the row below it are the neutrinos which are neutral. The antifermions' counterparts are not shown here, but all of these fermions have antiparticle counterparts. The boson columns displays the photon, the gluon, the positive and negative W bosons, the Z boson and the Higgs boson. The photon, gluon, Z boson, and Higgs boson do not have antiparticle counterparts, however the W^+ is the antiparticle of the W^-.

1 Background

1.1 Standard Model and PDFs

The Standard Model (SM) is an effective theory that describes the interaction of quarks and leptons with one another. There is a series of particles the SM describes, each with their own set of properties. Quarks and leptons, as described in Table (1), make up matter and interact via gauge bosons. The gauge bosons are the photon, the $W^{\pm}$ and Z boson, and the gluons, which mediate the electromagnetic force, the weak interaction, and the strong interaction, respectively. The SM is built using these three main forces, however it fails to describe gravity and is, consequently, an incomplete theory for all interactions in the universe. Even though this theory doesn't describe gravity, gravity is a very weak interaction so that its effect on the quantum

scale is negligible.

Each force has a corresponding *charge* which interacting particles must have. The electromagnetic interaction acts only on electrically charged particles. The weak interaction interacts on all particles. The strong interaction acts on particles that have *color charge*. The strong interaction is especially important because it gives a description of how hadrons, like protons and neutrons are made up of quarks.

The theory describing the quark and gluon interactions specifically is quantum chromodynamics (QCD). This sector of the SM is important in understanding the make up of hadrons since QCD dominates this bound state. Knowing the interaction of the quarks and the gluons (called partons) is not enough for a holistic understanding of hadrons. The wave function associated with the partons is decoherent, meaning that properties like the momentum of the partons aren't well known. A probability description is used to describe the partons making up a hadron. Parton distribution functions (PDFs) provide a probability-based description of the partons and work as a means of bridging interactions with hadrons to the more fundamental interaction of partons. There is currently no analytic means of determining PDFs. This is the importance of global fitting, like those found in the PDF sets like the Alekhin-Blümlein-Moch PDF set (ABM12), CTEQ-Jefferson Lab PDF set (CJ15), CTEQ-TEA PDF set (CT14), Neural Network PDF set (NNPDF30), etc. These efforts attempt to constrain the free parameters in models which provide a functional form for PDFs. Varying experiments with

large momentum transfers like deep inelastic scattering (DIS) and hadron-hadron collisions are very useful in adding constraints to these models. For more information on PDFs see Sec. (1.4).

1.2 Perturbation Theory and the Standard Model

The Standard Model has been used to accurately predict observables. These observables in the case of particle interactions in collider experiments are *differential cross sections*, $d\sigma$. A cross section, σ can be thought of as the probability of an interaction occurring. A cross section has units of area and, in the classical case, is a real cross section. For example, consider the case of a beam of light particles incident upon a hard spherical potential. A calculation for this system would yield a cross section of πr^2. Similar calculations can also be done for all types of interactions.

Differential cross sections are especially useful in collider physics. Classically or even quantum mechanically, if a beam of light charged particles were incident on a heavy charged particle, as in proton-electron scattering, the cross section would be infinite. This is a consequence of the Coulomb force having an infinite range since,implying that even at large distances the particles still interact. This infinity might seem troublesome, but information can still be gained from analysing differential cross sections. If one instead analysed the cross section of a set of particles scattered toward a differential solid angle, $d\Omega$, the result becomes finite. The differential cross section in the frame of the heavy scattering center, calculated using either quantum

7
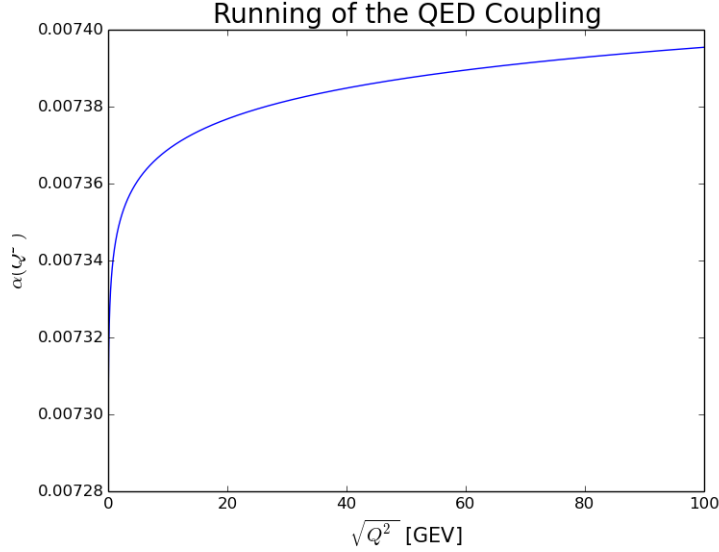
Figure 1: The running of the coupling associated with QED. Notice as $Q^2 \to 0$ the coupling is $\alpha(0) \approx \frac{1}{137}$.

mechanics with a Coulomb potential or classical Coulomb scattering, is

$$\frac{d\sigma}{d\Omega} = \frac{m^2 \alpha^2}{4p^4 \sin^4 \frac{\theta}{2}} \qquad (1)$$

where θ is the scattering angle and m and p are the mass and initial momentum of the electron. The constant α is the fine structure constant and is approximately $\frac{1}{137}$. The SM predicts higher order $\mathcal{O}(\alpha^3)$ terms in this cross section. The result shown in Eq. (??) is actually an approximation to the cross section predicted by quantum electrodynamics (QED). QED is a relativistic quantum theory of charged particles and photons and it is a part of the Standard Model. The higher order effects predicted by QED become important at higher energies, and can be calculated using pertur-

bation theory. A crucial requirement of perturbation theory for scattering is that there must be some perturbatively small factor associated with the interaction. The dimensionless quantity α is the perturbative factor for the electromagnetic interaction described above. This factor is sufficiently small for the usage of perturbation theory. Still there is an important fact neglected in this argument. The α shown above is actually a function of the momentum transfer, Q^2. The parameter Q^2 is defined as the negative of the Minkoswki product of the momentum transfer of the virtual photon incident on a charged particle. For our purpose, it is a measure of an energy characterizing a scattering process. Fair usage of perturbation theory requires that $\alpha(Q^2)$ is small for a given Q^2. Fortunately, for energy scales relevant to modern collider energies (10^4 GeV) the physical fine structure remains small, see Fig. (1).

The coupling in QCD, α_s, for small Q^2 is large i.e. $\alpha_s(0) \approx \mathcal{O}(1)$. This would seem to be a problem for using perturbation theory for QCD. However, due to the properties associated with QCD (see Sec. (1.3)) the coupling isn't a monotonically increasing function in $\sqrt{Q^2}$ as is the case for QED. Instead, it decreases and asymptotically approaching zero (see Fig. (2)). When the momentum transfer is near $\sqrt{Q^2} = 90$ GeV the constant is perturbatively small, $\alpha_s(90\,\text{GeV}) \approx 0.1185$. This is quite useful because perturbation theory can be used in QCD for energy ranges explored in modern collider experiments.
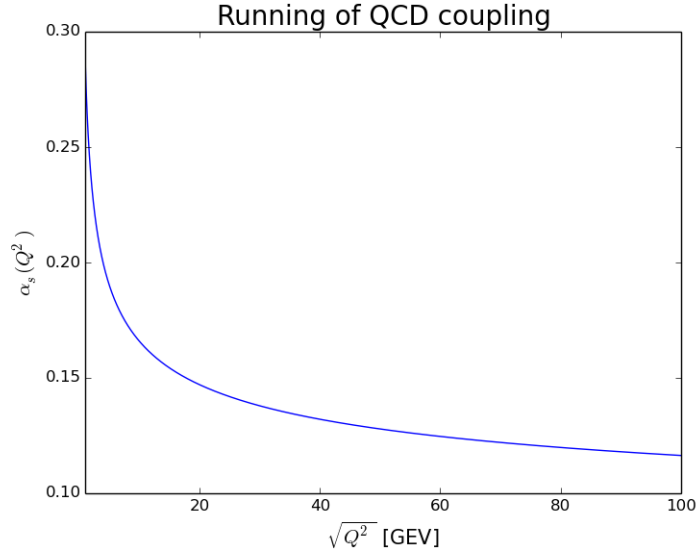
Figure 2: The running of the coupling for QCD.

1.3 Summary of Perturbative Quantum Chromodynamics

The properties of the strong interaction, in comparison to the electromagnetic interaction, are quite unfamiliar. There are more than just two charges in QCD, in fact, there are a total of six color charges. The color charges are red (r), green (g), blue (b), antired ($\bar{r}$), antigreen ($\bar{g}$), and antiblue ($\bar{b}$). The quarks carry the color charge and their counterparts, the antiquarks possess the anticolor charge. Gluons, the mediator of the strong interaction, also have color-anticolor charge. The gluon is the gauge boson of QCD, just as the photon is the gauge particle of QED. Photons are not electrically charged, so the gluon having color charge results in different properties for QCD. An important consequence of gluons having color charge is *color confinement.*

10

This means that hadrons, bound states dominated by QCD, cannot be color ionized. There is, again, no analogy in electromagnetism. An atoms, which is a bound state dominated by electromagnetism (EM), can be electrically ionized if it is given enough energy. Hadrons cannot be color ionized. This means that all final states must be color neutral, sometimes called white. Hadronisation is a direct consequence of this. A proton will create a jet of other hadrons (the sort of hadrons are constrained by conservation laws), but never will become a collection of disassociated partons. Equivalently, free quarks or gluons can never be directly observed. This would seems to imply that partons are strongly interacting in the final and initial state of a process. A lack of free particles in the final and initial states would make the calculation of cross sections very difficult, luckily partons are *asymptotically free*. This means that the partons can be treated as free in these bound states, only interacting strongly at higher length scales. Partons behaving freely on short distance scales is imperative in perfmoingin perturbative calculations.[1]

1.4 Parton Model in Deep Inelastic Scattering

Proton structure can be resolved at sufficiently high energy. A description of the form for the proton is given by structure functions. Structure functions,

---

[1]There are non-perturbative techniques that can be used for QCD calculation, most notably lattice QCD. Such technique are powerful for predicting low-energy-regime properties of hadrons. Lattice QCD famously, approximated the rest mass of the proton, a feat impossible for perturbative QCD. The downside of lattice QCD it that is numerically intensive. The aforementioned rest mass prediction required months of calculations on a super computer.
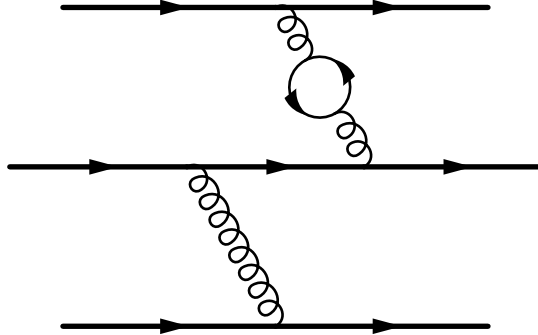
Figure 3: The gluon binding quarks together can produce quark-antiquark pairs. When particles interact with hadrons one must consider the quarks created from the gluon field. The bold line are the valence quarks while the lines in the loop represent the sea quarks.

even at fairly low energies, indicate the proton is not a point particle like the electron seems to be. In electron-proton DIS ($ep \to eX$), the structure functions enter the cross section[2] as

$$
\begin{aligned}
\frac{d\sigma}{d\Omega} &= \frac{\alpha^2}{4E^2 \sin^4 \frac{\theta}{2}} \frac{E'}{E} \{ (F_1^2 - \frac{E' - E}{2m_p} F_2^2) \cos^2 \frac{\theta}{2} \\
&- \frac{E' - E}{m_p} (F_1 + F_2)^2 \sin^2 \frac{\theta}{2} \}
\end{aligned}
\tag{2}
$$

E is the initial energy of the electron, E' is the final energy of the electron (which is fixed for this cross section) and $F_1(x, Q^2)$ and $F_2(x, Q^2)$ are the structure functions. If $F_1 = 1$ and $F_2 = 0$, this would correspond to a point particle.

In DIS the collider energy is much greater than the mass of the proton. The electron, acting as a probe, has enough energy to resolve the structure of the proton. At the same time, the electron has enough energy to change the proton into jet of other hadrons. The parton paradigm implies the con-

---

[2] In the frame of an initially at rest proton and in the limit of a massless electron.

stituents carry some fraction of the momentum of the proton, ξ, or

$$p_q = \xi p_P \tag{3}$$

here p_q is the momentum of the quark and p_P the momentum of the proton. The momenta of the partons aren't easily observable due to the difference in time-scales of the partons, $\frac{1}{m_p}$, and time scale of the collider, $\frac{1}{\sqrt{Q^2}}$.[3] Since the partons are "hidden" inside of the initial proton, the exact momenta of the partons cannot be determined. However, a probability distribution can be used. This probability density function will give the probability of interacting with one of the inner partons carrying some momentum fraction between ξ ad $\xi + d\xi$. The probability is $f_i(\xi)d\xi$, where i denotes the particular species of the parton. The function $f_i(\xi)$ is the Parton Distribution Function (PDF). Of the six flavours of quarks that can make up the proton, the main flavours are the up and down quarks. Naively, one would say that the proton is made up of two up quarks and one down quark alone. This idea is simplified only because it ignores the importance of the gluon which carry half around half of the momentum of the proton. Since there is a chance for the gluon to produce quark-antiquark pairs (as shown in Fig. (3)) the structure of the proton is not so simple. Quarks originating from the gluon field are called the *sea quarks* while the "naive quarks" are called the *valence quarks*. The

---

[3]Natural units are used here:

$$\hbar = c = \epsilon_0 = \mu_0 = 1$$

probability for finding a particular species of quarks is given by the evaluation of an integral of the PDF over a momentum fraction spanning from 0 to 1. Due to the gluon creating the quark-antiquark pairs in equal amounts one must subtract the antiquark PDFs to get to the appropriate number. So this looks like

$$
\int_0^1 d\xi(f_u(\xi) - f_{\bar{u}}(\xi)) = 2
$$
$$
\int_0^1 d\xi(f_d(\xi) - f_{\bar{d}}(\xi)) = 1 \tag{4}
$$
$$
\int_0^1 d\xi(f_s(\xi) - f_{\bar{s}}(\xi)) = 0
$$

$$
...
$$

or more generally

$$
\int_0^1 d\xi(f_q(\xi) - f_{\bar{q}}(\xi)) = N_q \tag{5}
$$

where N_q is the number of quarks of flavour q.

Another constraint can be derived from the conservation of momentum. First say that the momentum of the proton is the classical sum of all of the momenta for each species of quark, then

$$
\sum_i N_i p_i = p_P
$$
$$
\sum_i \int_0^1 d\xi f_i(\xi) \frac{p_i}{p_P} = 1 \tag{6}
$$
$$
\sum_i \int_0^1 d\xi f_i(\xi)\xi = 1
$$

where i denote quark, antiquark and gluon species. This is simply the conservation of momentum written in terms of the PDF of the quarks. These are important conservation laws that are used in the determination of the PDFs.

Now with these probability functions, in hand one can write the proton's cross section in terms of the partonic cross sections. This is

$$\sigma = \sum_i \int_0^1 d\xi f_i(\xi)\sigma_i \tag{7}$$

Each quark is assumed to be a free point particle inside of the proton, so we can write a particular parton species', i, interaction with an electron in DIS as

$$\frac{d^2\sigma_i}{d\Omega dE'} = \frac{\alpha^2 Q_i^2}{4E^2 \sin^4 \frac{\theta}{2}}(\cos^2 \frac{\theta}{2} + \frac{Q^2}{2m_q^2}\sin^2 \frac{\theta}{2})\frac{2m_p x^2}{Q^2}\delta(\xi - x) \tag{8}$$

letting Q_i denote the charge of the quark and

$$Q^2 = 2m_q(E' - E)$$

The parameter x is often called the Bjorken variable and E is the energy of the incident electron. Note the similarity of Eq. (8) to Eq. (2). Now Eq. (7) and Eq. (8) imply that the cross section for the proton in DIS in terms of the cross section of the partons are

$$\frac{d\sigma}{d\Omega dE'} = \sum_i f_i(x)\frac{\alpha^2 Q_i^2}{4E^2 \sin^4 \frac{\theta}{2}}(\frac{2m_p x^2}{Q^2}\cos^2 \frac{\theta}{2} + \frac{1}{m_p}\sin^2 \frac{\theta}{2}) \tag{9}$$

15
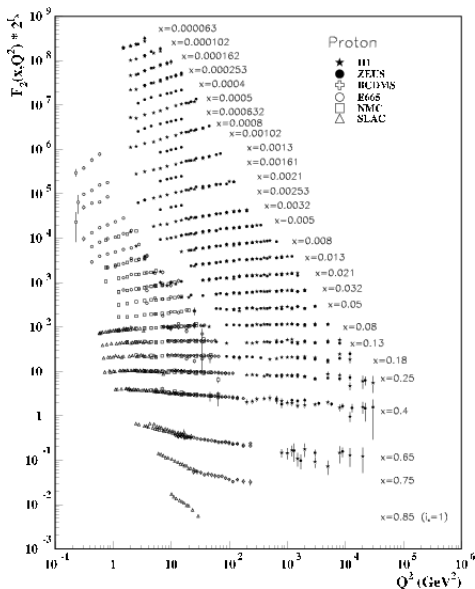
Figure 4: Experimental verification of the Bjorken scaling phenomenon. Notice that F_2, one of the structure functions associated with the proton, has very little dependence on Q^2. Logarithmic dependence arises from higher order QCD effects.

Using this gives insight onto the form of the structure function in Eq. (2). The structure functions are

$$2xF_1(x, Q^2) = F_2(x, Q^2) = x \sum_i Q_i^2 f_i(x) \tag{10}$$

This result after some analysis yields two important facts: Bjorken scaling and the Callan-Gross relation. The Bjorken scaling states the structure functions at leading order are independence of Q^2. Bjorken scaling is a statement of protons being made of point particles. Bjorken scaling was also seen experimentally as shown in Fig. (4). This independence is approximate and has some small logarithm dependence that originates from QCD higher order effects. The dependence on Q^2 is determined by a set of PDF evolution

16
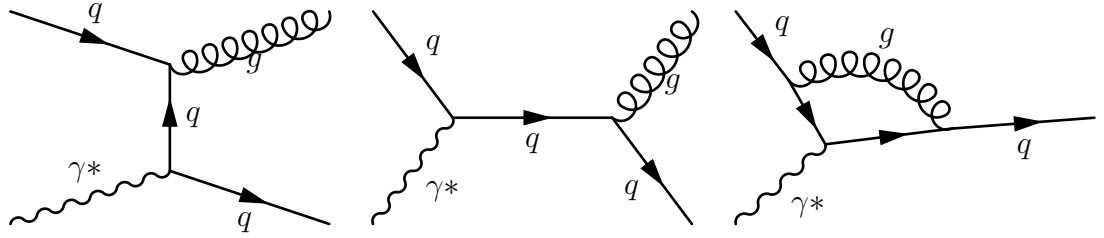
Figure 5: Some of the QCD corrections used in the consideration of the Q-dependence of DIS. The incoming photon is the virtual photon associated with the DIS process.

equations called the DGLAP equations. The second result, the Callan-Gross relation, is

$$F_2(x, Q^2) = 2x F_1(x, Q^2) \tag{11}$$

which implies that the spin statistic of the quark are the same as that of the proton. So the quarks are spin-$\frac{1}{2}$ Dirac fermions.

Knowing Eq. (9) isn't enough. Beside this being a leading order calculation it doesn't include the possibility for the initial state partons to scatter inelastically into other quarks and gluons. This would require higher order QCD calculations, as mentioned previously, which give the DGLAP evolution equations and splitting functions. It involves the scattered quark emitting a gluon or absorbing a gluon, and the gluons changing into quark-antiquark pairs. Some of the QCD diagrams are shown in Fig. (5). This result, in conjunction with a fragmentation function [4] predict phenomena seen in collider experiments.

DIS is a strong tool for understanding the constraints that one can imple-

---

[4]Fragmentation function are the opposite of PDF's. PDF's relates the quark's cross section to the proton's, while the fragmentation function relate the scattered produces quark and gluons to final state hadrons.

ment on PDFs. The up and down quark PDFs can be understood well, due to their large presence in targets (e.g. proton and nuclei). DIS experiments are important data sets to help in the determination of PDFs. Neutrino beam are also utilized in experiments. The neutrino-nuclear experiments are also especially useful in determination of the strange PDF. However, DIS has some limitation. The beams used are typically a beam of leptons scattering with some nuclear target. Since leptons don't strongly interact with gluons, the gluon PDFs must be determined with a different process. The nuclear target experiments also require off-shell nuclear correction since the proton and neutrons are in a bound state and do not assume their usual masses. Secondly, the scatter quark must propagate through a nuclear medium, resulting in difficult correction terms. Hadron-Hadron experiments conducted at accelerators like the LHC and at the Tevatron are useful tool in exploring other forms of constraints on PDFs with no issues associated with nuclear effects. The experiments also have the benefit of higher energies.

1.5 Hadron-Hadron with Drell-Yan or Vector Boson Interactions

Hadron-hadron collisions are often able to get to much higher center-of-mass energies than DIS collisions.[5] The collision between two hadrons involve an extra degree of freedom due to uncertainty in the energy of the interacting

---

[5]Higher mass charged particles do not radiate energy as much as lower mass particles, so an electron cannot easily be accelerated to high energies, unlike a proton.

partons. This results in a requirement for three variables, unlike the two in DIS e.g. E' and Ω or one in elastic scattering e.g Ω. One set of variables that could be used is the momentum transfer Q^2, the momentum fraction of the first interacting parton x_1, and the momentum fraction of the parton from the second hadron x_2 (it doesn't matter which hadron is designated as "first"). However, since the momentum fractions aren't observable they need to be related to a set of experimentally well-measured quantities. These are

$$y = \frac{1}{2} \ln \frac{x_1}{x_2}$$
$$M^2 = x_1 x_2 s$$

(12)

where s is one of the Mandelstam variable associated with the total center of mass energy of a collision. It, formally, is the Minkowski squared of the sum of the four-momenta for the incoming hadrons.

$$s = (p_1 + p_2)^2$$

(13)

The variable M is the invariant mass of the process and y is the rapidity. Rapidity can be physically understood as a Lorentz-invariant formulation of angles. Rapidity is defined as

$$y = \frac{1}{2} ln(\frac{E + p_z}{E - p_z})$$

(14)

19
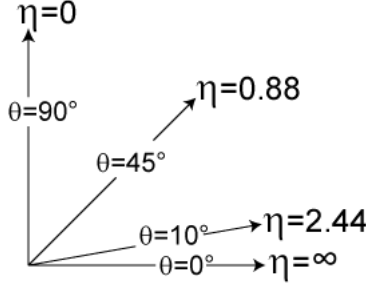
Figure 6: This shows the spatial dependence of the pseudorapity η. Notice, that going forward down the beam line indicated $\theta = 0$ and $\eta = \text{inf}$, while backwards along the beam line is $\theta = \pi$ and $\eta = -\text{inf}$. Directly perpendicular to the beam is $\theta = \frac{\pi}{2}$ and $\eta = 0$

where p_z is the longitudinal momentum. This formulation is convenient since the change in rapidity is invariant under a Lorentz-transform ($\Delta y' = \Delta y$). The invariance of the difference in momentum allows for calculations to be performed in different reference frame but retain the same bin size. In the $m \to 0$ limit, often the rapidity y is replaced with the pseudorapidity, η, which in terms of θ, is

$$\eta \equiv -\ln(\tan\frac{\theta}{2}) \tag{15}$$

See Fig. (6). The inverse transforms for Eq. (12) are

$$
\begin{aligned}
x_1 &= \frac{M}{\sqrt{s}}e^{y} \\
x_2 &= \frac{M}{\sqrt{s}}e^{-y}
\end{aligned}
\tag{16}
$$

Hadron-hadron processes are especially important since they are able to explore extremely high energies. For PDF constraints this allows for better fit at much lower x values, considering Eq. (16).

The Drell-Yan process is one that includes the interaction of a neutral

20

current as the mediator of a hadron-hadron interaction. This interaction could be an Z boson or a photon as seen in Fig. (7). Drell-yan processes are important for PDFs since they are sensitive to exotic distribution like the strange PDF. Weak vector boson production with $W^{\pm}$ is similarly helpful just as in the case for Drell-Yan processes. By examining data for these processes, one can find constraints on PDFs in terms of product of PDFs. A formulation can be investigated for another observable in weak vector boson interactions. If a W^- boson is inclusively selected in an experiment from lepton distributions (see Fig. (7)), the cross section that has PDFs dependent is[6]

$$
\begin{aligned}
\frac{d\sigma}{dy} &= (\cos^2\theta_c \bar{u}(x_1)d(x_2) + \sin^2\theta_c \bar{u}(x_1)s(x_2) \\
&+ \cos^2\theta_c \bar{c}(x_1)s(x_2) + \sin^2\theta_c c(x_1)d(x_2) + ... + (switch 1 \leftrightarrow 2))\frac{d\hat{\sigma}}{dy}
\end{aligned}
\tag{17}
$$

where θ_c is the Cabbibo angle and $\hat{\sigma}$ denotes the partonic cross section. This angle correspond to a 2×2 rotation matrix relating the interaction of u and c quarks to d and s. A more general form of the Cabbibo matrix is the Cabbibo-Kobayashi-Maskawa (CKM) matrix which contains the Cabbibo 2×2 in the

---

[6]This cross section is written in terms of the first and second generation quarks. These are the lightest quarks and contribute the most to these interactions.
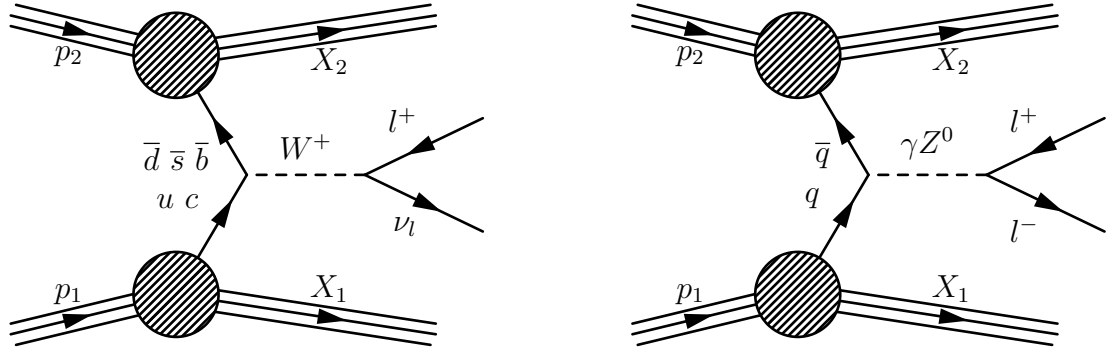
Figure 7: These are the Feynman diagrams representing the The Drell-Yan process at the LHC and the vector boson process with W^+. Drell-Yan is on the left and W production is on the right. The quarks shown in the figure can originate from either proton 1 or proton 2. There is another similar diagram including W^- production.

upper left corner. The CKM matrix is approximately

$$V_{qq'} \approx \begin{pmatrix} 1 & .2 & 0 \\ .2 & 1 & .2 \\ 0 & .2 & 1 \end{pmatrix} \tag{18}$$

where each row corresponds to the u, c, t quarks, respectively and each column corresponds to the d, s, b quarks, respectively. This matrix implies that some quark products are suppressed. At particularly low momentum fractions and high Q^2 the sea and the valence quark are comparable with one another, so the CKM factor can increase the sea quark contributions enough to help gain more information about exotic quark distributions. Observables, including the differential cross section for W^+, are sensitive to variations in the more exotic quark especially at higher energies, $\sqrt{s}$ and at higher rapidities, y.

22
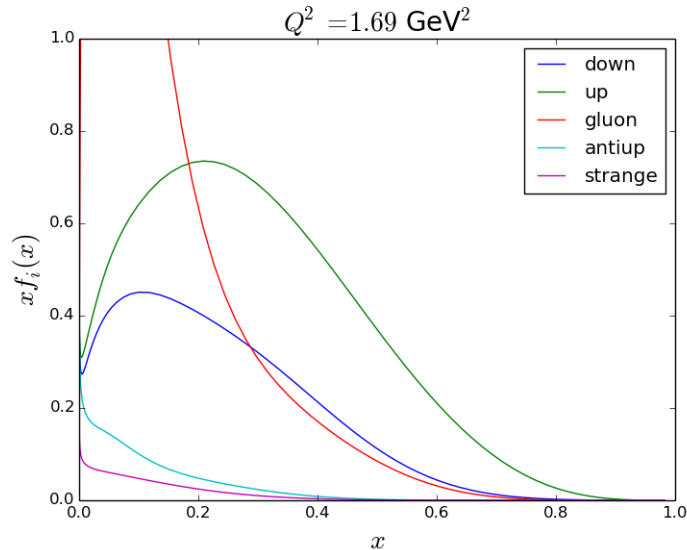
Figure 8: The original quarks distribution as described by the unchanged CJ15 PDF set. This is at a small momentum transfer of $Q^2 = 1.69$ GeV^2.

1.6 The CTEQ-Jefferson Lab (CJ15) PDF set

2 Global Fitting

2.1 Parametrization

From DIS, and hadron-hadron collision, much has already been learned about the larger quark distributions of the proton. The up quark, the down quark, the antiup, the antidown and the gluon distribution are fairly well constrained. The heavier quark PDFs are less known. Since the exotic quarks have heavier masses and have no valence inside of the proton, these PDFs are smaller at moderate energies and rapidities in comparison to the up and down PDFs. Gluons more often produce sea quarks of lower masses like the
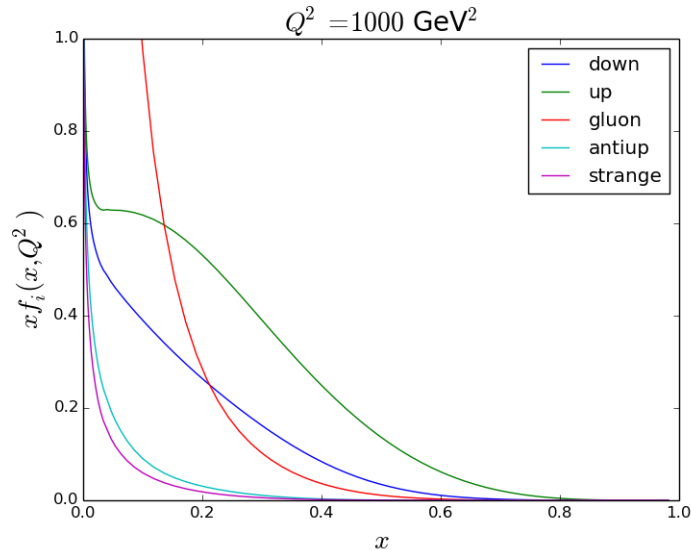
Figure 9: The original quarks distribution as described by the unchanged CJ15 PDF set.This is at a small momentum transfer of $Q^2 = 1000$ GeV^2.

u, $\bar{u}$, d and $\bar{d}$ quarks, but the higher mass quark are less likely. When the size of the PDFs are small it becomes difficult to discern the variation in quark PDFs from the theoretical and experimental uncertainty associated with constraining the PDFs from data. For this reason, one must search for data that is sensitive to exotic PDFs.

The lightest exotic quark is the strange quarks so, naturally, the PDF of interest to be constrained is the strange PDF. One of the assumption associated with the strange distribution is that the strange and the antistrange PDF are the same. This is an assumption originating from the matter-antimatter symmetry of the Standard Model and with the fact that gluons producing strange and antistrange quarks in equal amounts. This means the when fitting the strange PDF that the function that is being constrained is

24

in fact

$$\frac{s(x) + \bar{s}(x)}{2}$$

Another assumption is that the strange quark behaves similarly to the other sea quarks. This assumption is parametrized mathematically as

$$\frac{s(x) + \bar{s}(x)}{2} = \kappa \frac{(\bar{u}(x) + \bar{d}(x))}{2} \tag{19}$$

A more telling parametrization used in this analysis includes x-dependence,

$$\frac{s(x) + \bar{s}(x)}{2} = \kappa x^{\kappa_1} (1 - x)^{\kappa_2} \frac{(\bar{u}(x) + \bar{d}(x))}{2} \tag{20}$$

This parametrization is a simple and more general form that shifts the function and changes the general shape.

The starting point for the fitting done here is the CJ15 PDF set [1]. This PDF set used data originating from several different types of DIS and hadron collider experiment to fit free parameters in a PDF model. This PDF set used data sets from experiment HERA, JLAB, LHC, Tevatron etc. A visual representation of the CJ15 PDFs are shown in Fig. (8) and (9). The CJ15 PDF set avoided the fitting of data that involved heavy nuclei. This is due to the fact that a heavy nucleus contains bound protons and neutron instead of free nucleons. This implies that the nucleons are off-shell. When analysing processes involving a nucleus one must also consider the propagation of partons through a nuclear medium. These effects are not

completely understood and so there may be some discrepancy between PDFs of a free proton and these nuclear PDFs.

2.2   Chi-squared minimization

The global fitting program used here utilizes a χ^2 minimization technique to vary parameter associated the CJ15 parameters, including the addition new x-dependent variables for the strange quark PDF. The minimization algorithm reads in many data sets including the LHCb and CMS data sets. The global fitting program varied the parameter to explore a multidimensional parameter space, to find a point that minimizes the χ^2

$$\chi^2 = \sum_{i=1}^{N} \frac{(O_i - E_i)^2}{\sigma_i^2} \tag{21}$$

where O is the experimental observable and E is the theoretically expected value. The uncertainty, σ, is the error in the observed measurement. These observed and theoretical quantities are observables that are associated with a particular processes. When invoking calculations for, say the differential cross section $\frac{d\sigma}{dy}$, the variation is done on several parameters, minimizing the value of χ^2. Inside of the global fitting algorithm, there are LO calculation done for the lepton rapidity observable. The NLO calculation can be done with a simple K factor that originates from a Monte Carlo process calculator in the same region of kinematic space as the data used. The Monte Carlo Femtobarn process Measurement (MCFM) program is used for the calculation of K
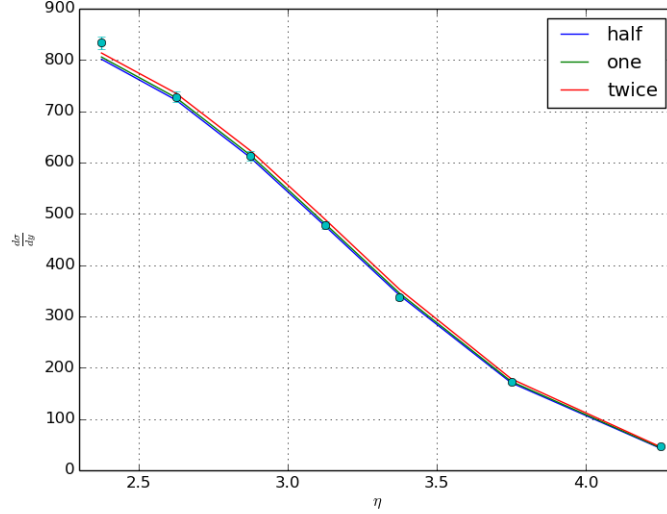
Figure 10: Plus distribution sensitivity. The sensitivity plot is made by doubling and halving the κ value in the normal CJ15 parametrization.

factors. K factors for a rapidity distribution are

$$K(y) = \frac{\frac{d\sigma_{NLO}}{dy}}{\frac{d\sigma_{LO}}{dy}} \tag{22}$$

By implementing a rapidity dependent K factor important theoretical NLO calculations can be approximated. Without this factor the theoretical value would unduly deviate from the observed value by 10%. This factor is especially important since the global fitting program might change a free parameter to compensate for the 10%, resulting in an unphysical result.

27
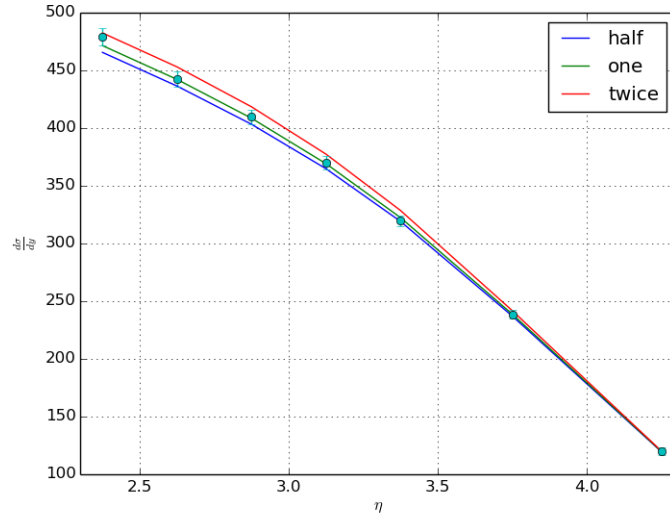
Figure 11: Minus distribution sensitivity. The sensitivity plot is made by doubling and halving the κ value in the normal CJ15 parametrization.
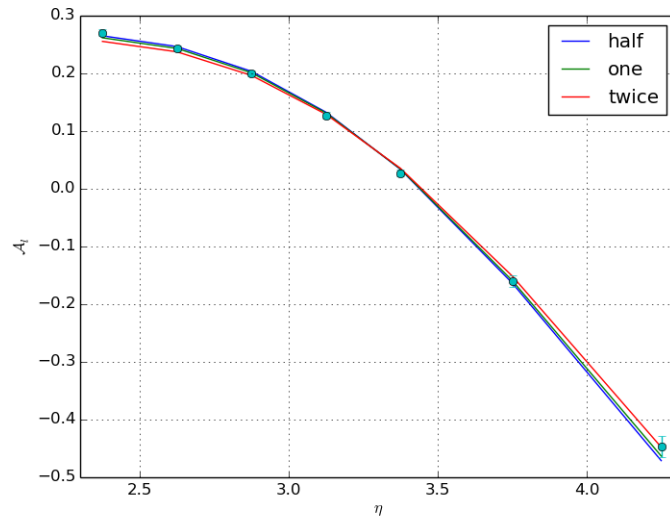
Figure 12: Lasy distribution sensitivity. The sensitivity plot is made by doubling and halving the κ value in the normal CJ15 parametrization.
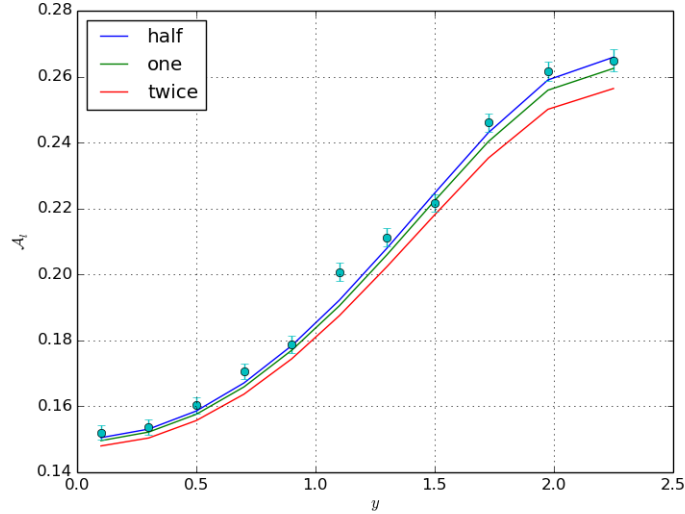
Figure 13: Lasy CMS distribution sensitivity. The sensitivity plot is made by doubling and halving the κ value in the normal CJ15 parametrization.

2.3 Additional Data sets

The new data sets which were added to the original CJ15 sets are from the CMS [2] and LHCb [3] detectors at the LHC. The original CJ15 data sets include measurements from the Tevatron, the ATLAS detector at LHC, SLAC, among others. All of these measurement along with the new data were included in the global fits.

2.3.1 CMS

The CMS (Compact Muon Solenoid) detector is an apparatus armed with several layers of detecting materials. These include the silicon tracker, the pixel tracker, the electromagnetic calorimeter, and the hadronic calorimeter.

These detecting elements with particle flow algorithms allow the CMS detector to understand what sort of particles are created from proton-proton collisions.

The CMS data used here includes data from rapidity ranging from -2.4 $< \eta <$ 2.4 with a center-of-mass energy $\sqrt{s} = 7$ TeV. The observable tested here is the lepton asymmetry. An important cut made to the data is the requirement of the transverse momentum of the detected lepton being greater than 25 GeV, this cut is incorporated in the theoretical calculation as well. Lepton asymmetry taken experimentally is calculated with the number of particles in a particular rapidity bin Δy. The number of positively charged leptons is denoted by N_+ and the negatively charged leptons is denoted by N_-. So the lepton asymmetry with respect to rapidity is

$$\mathcal{A}_l(y) = \frac{N_+(y) - N_-(y)}{N_+(y) + N_-(y)} \tag{23}$$

Here the rapidity y, is the average of the bin width chosen. The data used is shown in Table (2). The theoretical lepton asymmetry is calculate as

$$\mathcal{A}_l = \frac{d\sigma(W^+ \to l^+\nu)/dy - d\sigma(W^- \to l^-\bar{\nu})/dy}{d\sigma(W^+ \to l^+\nu)/dy + d\sigma(W^- \to l^-\bar{\nu})/dy} \tag{24}$$

The data from the CMS detector is shown in table (2).

y	$\mathcal{A}_l(\text{Theory})$	$\pm$ error	$\mathcal{A}_l(\text{Exp.})$	$\pm$ error	χ^2
0.1000	0.1512	0.0007	0.1521	0.0023	-0.15
0.3000	0.1538	0.0007	0.1538	0.0023	0.00
0.5000	0.1594	0.0007	0.1603	0.0024	-0.15
0.7000	0.1679	0.0007	0.1706	0.0024	-1.28
0.9000	0.1792	0.0007	0.1788	0.0026	0.02
1.1000	0.1929	0.0007	0.2007	0.0028	-7.75
1.3000	0.2086	0.0008	0.2113	0.0027	-1.01
1.5000	0.2251	0.0008	0.2217	0.0027	1.61
1.7250	0.2430	0.0009	0.2461	0.0028	-1.22
1.9750	0.2583	0.0009	0.2616	0.0028	-1.43
2.2500	0.2644	0.0008	0.2649	0.0034	-0.02

Table 2: Data with theory output from global fitting program. Data from [2] is list in terms of rapidity y which is the same a pseudorapidity in the relativistic limit.

2.3.2 LHCB

The LHCb detector differs from the other detectors in the LHC series. It is designed to measure the relatively short-lived bottom hadron. To measure these short-lived particles the detector must measure very close to the beam line, since those hadrons have the most energy and time-dilation lengthen the tracks in the detector. This detector measures in the high forward rapidity, $2.0 < \eta < 4.5$. This new data is important to PDF calculations since one can now explore a lower momentum fraction. The higher rapidity range along with 8 TeV energies leads to a lower bound on the momentum fraction. The theoretical bound on the LHCb data, using Eq. (12), would be

$$x = \frac{M_W}{\sqrt{s}} e^{-\eta} \tag{25}$$

31

η	$\frac{d\sigma}{d\eta}$(Theory)	$\pm$ error	$\frac{d\sigma}{d\eta}$(Exp.)	$\pm$ error	χ^2
2.3750	801.6906	3.3966	833.6000	12.6870	-6.33
2.6250	722.2701	2.9997	728.0000	10.6730	-0.29
2.8750	610.0480	2.5137	613.2000	9.2090	-0.12
3.1250	477.1161	2.0024	478.0000	7.4730	-0.01
3.3750	342.1199	1.5357	337.6000	5.4990	0.68
3.7500	171.1682	0.9767	172.8000	3.1620	-0.27
4.2500	43.2217	0.4256	46.0000	1.6610	-2.80

Table 3: Positive rapidity distribution from LHCb detector [3].

or

$$x \approx \frac{90 \text{ GeV}}{8000 \text{ GeV}} e^{-4.5}$$
$$x \approx 10^{-4} \tag{26}$$

This gives a uniquely low x, not typically explorable by other detectors.

The new data sets included in this analysis are muon plus and minus rapidity distribution from LHCb [3]. The data sets are shown in tables (3), (4), and (5). The first data point ($y = 2.125$) in this analysis is removed, due to lack of theoretical agreement. Removal of this point from the data set leads to a significant lowering of the χ^2 by around 40 points. An important cut made to the data is the requirement of the transverse momentum of the detected lepton being greater than 25 GeV, this cut is incorporated in the theoretical calculation as well.

η	$\frac{d\sigma}{d\eta}$(Theory)	$\pm$ error	$\frac{d\sigma}{d\eta}$(Exp.)	$\pm$ error	χ^2
2.3750	467.0903	2.0338	479.2000	7.4300	-2.66
2.6250	438.3945	1.8680	442.4000	6.6930	-0.36
2.8750	405.4146	1.7156	409.6000	6.4620	-0.42
3.1250	366.7012	1.5672	370.0000	5.9460	-0.31
3.3750	320.5595	1.4057	319.6000	4.9800	0.04
3.7500	237.5447	1.1140	238.6000	3.8000	-0.08
4.2500	119.2534	0.6710	120.0000	3.6330	-0.04

Table 4: Minus rapidity distribution from LHCb detector [3].

η	$\mathcal{A}_l$(Theory)	$\pm$ error	$\mathcal{A}_l$(Exp.)	$\pm$ error	χ^2
2.3750	0.2637	0.0008	0.2702	0.0058	-1.25
2.6250	0.2446	0.0008	0.2439	0.0049	0.02
2.8750	0.2015	0.0008	0.1996	0.0049	0.15
3.1250	0.1309	0.0010	0.1274	0.0053	0.42
3.3750	0.0325	0.0014	0.0275	0.0060	0.69
3.7500	-0.1624	0.0024	-0.1599	0.0104	-0.06
4.2500	-0.4680	0.0039	-0.4463	0.0187	-1.35

Table 5: This is the list of data associated with the lepton asymmetry observable from the LHCb [3].
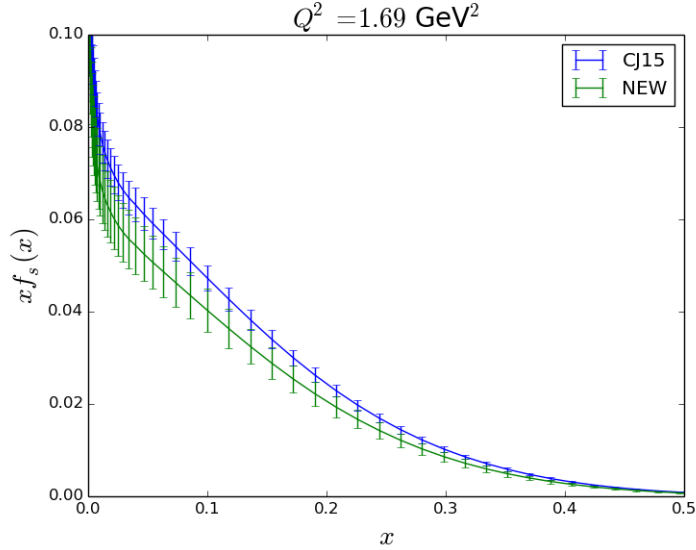
Figure 14: Comparison between the original CJ15 strange distribution and the new distribution from the added LHCb and CMS data.

2.4 Results

The CJ15 original strange quark parametrization is

$$s(x) = \kappa \frac{\bar{u}(x) + \bar{d}(x)}{2} \qquad (27)$$

This is the standard strange parametrization where the strange quark is assumed to be proportional to the antiup and antidown sa quarks. Originally in the previous CJ15 fit the value of κ was fixed to 0.4, which is supported from the CCFR DIS measurement. This parameter was not fitted since there lacked data sensitive to the strange quark distribution. The additional data sets can be added to the global fit data sets and new parametrization can be fitted. The data sets' observable's sensitivity to variation in the strange PDF is shown in figures (10), (12), (11), and (13). The variation in the observable is, in some cases, larger than the experimental error. This is an indication of a large enough sensitivity to variation in the strange quarks. So these are indeed sensitive observables to explore constraint for the strange quark. The parametrization used in this analysis is

$$s(x) = \kappa \frac{(\bar{u}(x) + \bar{d}(x))}{2}(1 - x)^{\kappa_1} x^{\kappa_2} \qquad (28)$$

This new parametrization of the strange quark is more general than the previous one in Eq. (27). With addition of κ_1 and κ_2 the strange distribution can be shifted towards low x or high x. Fitting κ, κ_1, and κ_2 and free all
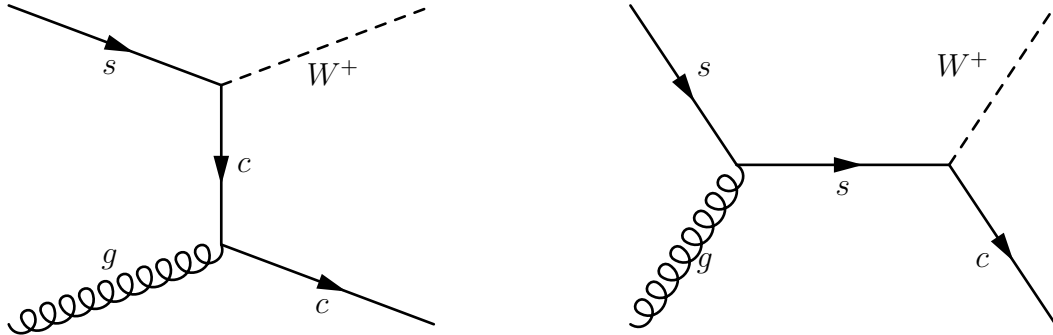
Figure 15: The leading order $\mathcal{O}(\alpha_s \alpha_w)$ partonic Feynman diagram for $W + c$ in the final state at the LHC. Similar diagrams can be constructed for the antistrange quark in the initial state.

the other CJ15 parameters lead to a new strange distribution shown in Fig. (14). The parameters are fitted to

$$\kappa = 0.33 \pm 0.038913$$

$$\kappa_1 = 8.3 \pm 3.7056 \tag{29}$$

$$\kappa_2 = -0.097 \pm 0.10204$$

Overall, the distribution is pulled down, and this is primarily due to the CMS data (see Fig. (14)). Still the errors on the new distribution are too large to give a definitive answer. The parameter κ_1 may indicate some x dependence but more research and more data is required to confirm this result.

2.5 Future works

In order to gain constraints on the the strange quark PDF, one must analyse more data sensitive to the strange quarks distribution. Analysis of vector boson production at the LHC with high rapidity and high center or mass en-

ergy would be a possible next step in determining constraints. With 13 TeV data being collected, the strange quark and other PDFs can be constrained in a small x region. More accurate NNLO calculations can also be implemented inside the global fitting program to increase the accuracy of certain calculations.

Another process one could test is the $W + c$ in the final state at the LHC. This process is shown in Fig. (15). This process favours a strange quark in the initial state due to the CKM matrix suppressing down quarks in the final state. A similar process prior to $W + c$ at LHC was measured at neutrino-iron nucleus experiments. Such experiments involved nuclei, so constraints would be determined for nuclear PDFs instead of for free nucleons. Usage of $W + c$ provides an opportunity to fit data sensitive to the strange quark without worrisome nuclear effects. Still a process like this is numerically intensive due to there being three particle in the final state (after the W bosons decay). This requires an integration over three phase spaces, one for each particle.

2.6   Conclusion

With the addition of data from the CMS [2] and LCHb [3] detectors there is support for lowering κ from 0.4 to around 0.33. The x-dependent parametrization involving $(1 - x)^{\kappa_1}$ is supported by a non-zero value for κ_1. The errors are large so more research should be done to understand this parametrization of the strange PDF. Implementation of the x^{κ_2} factor in the parametrization of the strange PDF is not well supported since κ_2 remained near zero. The

next step in determining constraints for the strange PDF could be found in including $W + c$ data from the LHC in the global fit.

References

[1] A. Accardi, L. T. Brady, W. Melnitchouk, J. F. Owens, and N. Sato. Constraints on large-x parton distributions from new weak boson production and deep-inelastic scattering data. *Phys. Rev.*, D93(11):114017, 2016.

[2] Serguei Chatrchyan et al. Measurement of inclusive W and Z boson production cross sections in pp collisions at $\sqrt{s} = 8$ TeV. *Phys. Rev. Lett.*, 112:191802, 2014.

[3] Roel Aaij et al. Measurement of forward W and Z boson production in pp collisions at $\sqrt{s} = 8$ TeV. *JHEP*, 01:155, 2016.

[4] Georges Aad et al. Measurement of $W^{\pm}$ and Z-boson production cross sections in pp collisions at $\sqrt{s} = 13$ TeV with the ATLAS detector. 2016.

[5] S. Alekhin, J. Bluemlein, S. Moch, and R. Placakyte. Iso-spin asymmetry of quark distributions and implications for single top-quark production at the LHC. 2015.

[6] V. Barger and R. Philips. *Frontier in Physics:Collider Physics*. Westview Press, 2 edition, 12 1996.

[7] Matteo Cacciari, Gavin P. Salam, and Gregory Soyez. The Anti-k(t) jet clustering algorithm. *JHEP*, 04:063, 2008.

[8] Serguei Chatrchyan et al. Measurement of the Rapidity and Transverse Momentum Distributions of Z Bosons in pp Collisions at $\sqrt{s} = 7$ TeV. *Phys. Rev.*, D85:032002, 2012.

[9] H. Goldstein, C. Poole, and J. Safko. *Classical Mechanics, 3rd ed.* Pearson, 3 edition, 6 2001.

[10] A. L. Kataev. The Gottfried sum rule: Theory versus experiment. In *Particle physics in laboratory, space and universe. Intelligentsia and education. Proceedings, 11th Lomonosov Conference on elementary particle physics, Moscow, Russia, August 21-27, 2003, and 5th International Meeting on problems of intelligentsia, Moscow, Russia, August 27, 2003*, pages 194–200, 2003.

[11] Vardan Khachatryan et al. Measurements of Inclusive W and Z Cross Sections in pp Collisions at $\sqrt{s} = 7$ TeV. *JHEP*, 01:080, 2011.

[12] J. F. Owens, A. Accardi, and W. Melnitchouk. Global parton distributions with nuclear and finite-Q^2 corrections. *Phys. Rev.*, D87(9):094012, 2013.

[13] M. Peskin and D. Schroeder. *An Introduction to Quantum Field Theory.* Westview Press, 1 edition, 6 2005.

[14] M. Schwartz. *Quantum Field Theory and the Standard Model.* Cambridge University, 1 edition, 12 2013.

[15] M. Thomson. *Modern Particle Physics.* Westview Press, 1 edition, 2013.